DOI:
10.1021/acsbiomaterials.9b01240

Document Version
Peer reviewed version

Controlled Release and Delivery Systems

Bioinspired Polymerization of Quercetin to Produce a Curcumin-loaded Nanomedicine with Potent Cytotoxicity and Cancer Targeting Potential In Vivo

Suhair Sunoqrot, Tahany Al-Debsi, Eveen AL-Shalabi, Lina Hasan, Farid Nazer Faruqu, Adam Walters, Robert G. Palgrave, and Khuloud T Al-Jamal

ACS Biomater. Sci. Eng., **Just Accepted Manuscript** • DOI: 10.1021/acsbiomaterials.9b01240 • Publication Date (Web): 18 Oct 2019

Bioinspired Polymerization of Quercetin to Produce a Curcumin-loaded Nanomedicine with Potent Cytotoxicity and Cancer Targeting Potential In Vivo

Suhair Sunoqrot[ab]*, Tahany Al-Debsi[a], Eveen Al-Shalabi[a], Lina Hasan[a], Farid Nazer Faruqu[b], Adam Walters[b], Robert Palgrave[c], and Khuloud T. Al-Jamal[b].

[a]*Department of Pharmacy, Faculty of Pharmacy, Al-Zaytoonah University of Jordan, Amman 11733, Jordan*

[b]*Institute for Pharmaceutical Science, King's College London, London SE1 9NH, UK*

[c]*Department of Chemistry, University College London, London WC1H 0AJ, UK*

***Corresponding Author:**

Suhair Sunoqrot, PhD

Associate Professor of Pharmaceutics

Department of Pharmacy

Faculty of Pharmacy

Al-Zaytoonah University of Jordan

P.O. Box 130, Amman 11733, Jordan

Phone: +962-6-4291511 Ext. 197

Fax: +962-6-4291432

Email: suhair.sunoqrot@zuj.edu.jo

Abstract

Nanomedicine has had a profound impact on the treatment of many diseases especially cancer. However, synthesis of multifunctional nanoscale drug carriers often requires multistep coupling and purification reactions, which can pose major scale-up challenges. Here we leveraged bioinspired oxidation-triggered polymerization of catechols to synthesize nanoparticles (NPs) from the plant polyphenol quercetin (QCT) loaded with a hydrophobic anti-cancer drug, curcumin, and functionalized with poly(ethylene glycol) (PEG) for steric stabilization in one reaction step. NPs were formed by base-catalyzed oxidative self-polymerization of QCT in the presence of curcumin and thiol-terminated PEG upon mixing in a universal solvent (dimethyl sulfoxide), followed by self-assembly with the gradual addition of water. Dynamic light scattering and X-ray photoelectron spectroscopy were used to confirm NP PEGylation. Drug loading was verified by UV-Vis spectroscopy. Curcumin-loaded NPs were efficiently internalized by CT26 murine colon cancer cells as determined by flow cytometry and confocal microscopy. NPs also demonstrated sustained release and potent cytotoxicity in vitro. Moreover, in vivo imaging of CT26 tumor-bearing Balb/c mice following tail vein injection of DiR-labeled QCT NPs showed steady tumor accumulation of the NPs up to 24 h. This was further supported by significant tumor uptake of curcumin-loaded QCT NPs as measured by flow cytometry analysis of tumor homogenates. Our findings present a greener synthetic route for the fabrication of drug-loaded surface functionalized NPs from poorly water-soluble plant polyphenols such as QCT as promising anti-cancer delivery systems.

Keywords: Quercetin; curcumin; bioinspired nanoparticles; cancer targeting; green chemistry

Introduction

Cancer is a leading cause of death worldwide, responsible for 9.6 million deaths in 2018.[1] Nonspecific uptake of small molecule anti-cancer drugs, which often results in severe side effects, can potentially be mitigated by nanoscale drug carriers.[2-4] Among the various types of nanocarriers available, a common denominator is the fact that the nanocarrier surface needs to be modified in order to impart functionalities such as prolonged in vivo half-life, reduced immunogenicity, and selective cellular targeting.[5-6] Surface modification techniques typically involve chemical conjugation of the desired ligand to the nanocarrier individual components before formation,[7-8] or conjugation to preformed nanocarriers using reactive linkers or coupling agents.[9-10] These techniques may also require exhaustive purification processes, which can be lengthy and inefficient and must be tailored for each ligand. The additional synthetic steps required can also lead to increased costs and greater regulatory hurdles.

Naturally-occurring polyphenols have attracted considerable attention in the past decade due to their unique features as biocompatible coating precursors for two- as well as three-dimensional surfaces.[11] Polyphenols such as dopamine, pyrogallol, tannic acid, and green tea catechins can undergo spontaneous oxidation and subsequent polymerization in aqueous alkaline buffers, forming stable surface coatings onto a wide range of substrates. This oxidative coupling process is inspired by naturally-occurring phenomena such as browning of polyphenol-rich fruits and vegetables upon air exposure as well as underwater adhesion of marine organisms such as mussels.[11-13] For example, Lee et al. used dopamine self-polymerization to form thin, surface-adherent polydopamine films onto various organic and inorganic materials, such as polymers, metals, semiconductors, and ceramics.[14-15] Li et al. synthesized polyphenol-coated mesoporous silica nanoparticles as a scaffold for immobilization of targeting moieties such as aptamers.[16]

Abouelmagd et al. reported tannic acid (TA) as an optically inert coating precursor for polymeric NPs, enabling the surface incorporation of albumin, chitosan, and folate-terminated PEG.[17] Polyphenol-mediated surface functionalization is facilitated by the reactivity of oxidized catechol moieties toward nucleophiles such as amine- and thiol-bearing ligands, in addition to noncovalent (H-bonding, hydrophobic, π-π stacking) interactions and metal chelation.[18] These features have inspired the development of standalone NPs as potential drug delivery nanocarriers, with the additional advantage of facile surface modification with desired ligands by relying on the reactivity of the oxidized catechols without using complex coupling reagents. Such polyphenol NPs have been reported using dopamine[19-20] and green tea polyphenols.[21-23]

We have recently devised a green NP synthesis technique by leveraging oxidation-triggered self-polymerization of the abundant plant polyphenol quercetin (QCT) in an aqueous alkaline buffer.[24] We showed that spontaneous oxidation of QCT at basic pH led to a series of coupling reactions and self-assembly, producing colloidal aggregates that could be functionalized with surface ligands (amine-terminated poly(ethylene glycol) (PEG)), and a small molecule anti-cancer drug (doxorubicin (DOX)). PEGylation and drug loading were facilitated by the reactivity of QCT's oxidized catechol moieties toward nucleophiles, and the ability to form H-bonding and π-π stacking interactions with DOX. Drug-loaded NPs exhibited high loading capacities, prolonged release, and potent anti-cancer activity.

Our QCT-based multifunctional NP platform was synthesized at ambient conditions without the use of any coupling reagents, and the purification process only involved ultrafiltration. However, the first-generation NPs were synthesized under aqueous conditions, which only allowed the incorporation of water-soluble drugs such as DOX. In addition, NP synthesis, surface functionalization, and drug loading were performed in sequential steps over several days, which

may be inefficient for future scale-up efforts. For these reasons, we developed a more simplified one-pot procedure that would allow QCT polymerization and simultaneous incorporation of surface ligands and poorly water-soluble cargo. We postulated that oxidative self-polymerization of QCT can be induced in an organic solvent such as dimethyl sulfoxide (DMSO) by the presence of a strong base, rendering the oxidized catechol moieties of QCT reactive toward a nucleophilic ligand such as thiol-terminated PEG. The synthesized "amphiphile" of PEG-QCT oligomers would then form colloidal assemblies upon the addition of water, with PEG chains exposed outward to impart steric stability in vitro and in vivo.[25-28] We further postulated that by adding a hydrophobic drug to the reaction mixture in DMSO, the former would become entrapped in the NP core during self-assembly, forming a PEGylated drug-loaded nanocarrier. Curcumin (CUR) was chosen as a model hydrophobic drug molecule for its reported anti-cancer, anti-oxidant, anti-microbial, anti-inflammatory, and neuroprotective properties.[29-36] It is also characterized by a polyphenolic structure, which would facilitate loading into QCT NPs, and intrinsic fluorescence that would enable NP tracking in vitro and in vivo.

NPs were characterized by dynamic light scattering (DLS) and scanning electron microscopy (SEM) to verify their size and morphology. Surface PEGylation was confirmed by Fourier transform-infrared (FT-IR) spectroscopy, surface charge measurements, and X-ray photoelectron spectroscopy (XPS). CUR loading and release, cellular uptake, and cytotoxicity experiments in a colon cancer model supported the viability of the one-pot method to produce functional CUR-loaded NPs with potent anti-cancer activity. Finally, passive targeting of the NPs in tumor-bearing mice was investigated by in vivo imaging and flow cytometry, further validating the potential of the newly designed NPs as an anti-cancer nanomedicine.

Experimental Section

Materials

Quercetin (QCT), curcumin (CUR), aluminum chloride ($AlCl_3$), sodium methoxide (NaOMe), 3-(4,5-dimethyl-2-thiazolyl)-2,5-diphenyl-2H-tetrazolium bromide (MTT), and hydrochloric acid (HCl, 10 M) were obtained from Sigma-Aldrich (St. Louis, MO, USA). Methoxy poly(ethylene glycol)-thiol, MW 5000 (mPEG-SH) was obtained from Laysan Bio (Arab, AL, USA). Dimethyl sulfoxide (DMSO), triethylamine (TEA), and Tween 20 were obtained from Tedia (Fairfield, OH, USA). 1,1'-dioctadecyl-3,3,3',3'-tetramethylindotricarbocyanine iodide (DiR) was obtained from Invitrogen (Thermo Fisher Scientific, Waltham, MA, USA). Phosphate buffered saline 10X (PBS) was obtained from Biowest (Nuaillé, France). Ultrapure water (~18.2 MΩ.cm) was prepared using a Millipore Direct-Q 5UV system (EMD Millipore, Billerica, MA, USA).

Synthesis of CUR-loaded QCT NPs

CUR-loaded QCT NPs (QCT@CUR NPs) were synthesized by base-catalyzed oxidative self-polymerization of QCT as previously described with some modification.[24] In a typical procedure, QCT (10 mg, 0.033 mmol; from a 50 mg/mL stock solution in DMSO) was mixed with different amounts of CUR (from a 20 mg/mL stock solution in DMSO) in a 20 mL glass vial protected from light, and the volume was completed to 1 mL with DMSO. The solution was vortexed to ensure complete dissolution and then placed on a magnetic stirring plate (Velp Arex, Usmate, Italy) at 500 rpm speed. TEA (9.2 μL, 0.066 mmol) was immediately added and the solution was stirred at room temperature (RT) overnight protected from light. The next day, ultrapure water (3 mL) was added dropwise to the DMSO solution under stirring at 500 rpm to induce NP self-assembly. After mixing for 1 h, the NP dispersion was transferred to a dialysis membrane (12 – 14 kD

MWCO, Spectrum Laboratories Inc., Rancho Dominguez, CA, USA) and dialyzed against deionized water for two days, with repetitive changing of the water, to remove DMSO, unreacted species and unentrapped drug. NPs were later centrifuged (1840 × g, 5 min; Hermle Z230A centrifuge, Wehingen, Germany) to remove any precipitates of unentrapped CUR. Drug-free QCT NPs were prepared as described above without the addition of CUR. PEGylated NPs were prepared by adding mPEG-SH (50 mg, 10 mM) to the DMSO solution after adding QCT and CUR but before the addition of TEA. DiR-labeled NPs were prepared by mixing QCT (10 mg), DiR (0.1 mg), and mPEG-SH (50 mg) in 1 mL DMSO and then adding TEA (9.2 μL). NP formation and purification was performed as described for CUR-loaded NPs. The composition of the different NP formulations is detailed in Table 1. NPs were lyophilized as needed using a FreeZone 4.5 L Benchtop Freeze Dryer (Labconco Corporation, Kansas City, MO, USA).

NP characterization by dynamic light scattering (DLS)

DLS was employed to measure the particle size and zeta potential of the prepared NPs using a Nicomp Nano Z3000 instrument (Particle Sizing Systems, Santa Barbara, CA, USA). Freshly prepared NPs diluted in ultrapure water were used for the analysis. Each measurement was performed in triplicate.

FT-IR and UV-Vis spectroscopy

FT-IR spectroscopy was performed using an IR Affinity-1 spectrometer (Shimadzu, Kyoto, Japan), where lyophilized samples were prepared as KBr discs. UV-Vis spectroscopy (Shimadzu UV-1800 spectrophotometer, Kyoto, Japan) was used to ascertain the presence of free –OH groups in QCT and QCT NPs using NaOMe and $AlCl_3$/HCl as previously described.[24, 37-38] Briefly, two

sets of methanolic solutions of QCT and QCT NPs were prepared at 10 μg/mL and their spectra were recorded. Spectra were then recorded immediately after adding NaOMe (1 M in methanol, 3 drops) to one of the sample sets, and $AlCl_3$ (50 mg/mL in methanol, 6 drops) to the second set. The spectra were also recorded immediately after adding HCl (5 M, 3 drops) to the $AlCl_3$ samples.

Scanning electron microscopy (SEM) and transmission electron microscopy (TEM) imaging

For SEM, a drop of PEGylated CUR-loaded QCT NPs (QCT@CUR@PEG NPs) suspended in ultrapure water was placed on double-sided carbon tape mounted on an aluminum stub and left to dry overnight prior to imaging using the SEM mode of a Versa 3D microscope (FEI, Netherlands) at 2 kV accelerating voltage and 10 mm working distance. For TEM, a drop of NPs suspended in ultrapure water was placed on Formvar-coated copper grids (300 mesh, Electron Microscopy Sciences, Hatfield, PA, USA) for 1 min, and the excess liquid was blotted with filter paper prior to imaging using the TEM mode on a Versa 3D microscope at an accelerating voltage of 30 kV and 10 mm working distance.

Calculation of drug loading and loading efficiency

CUR loading was measured by UV-Vis after diluting 100 μL of the NPs dispersed in water with 900 μL DMSO and recording the absorbance at 430 nm, based on a standard curve of CUR absorbance vs. concentration in DMSO at 430 nm. Each measurement was performed in triplicate. Drug loading and loading efficiency were calculated according to Equations (1) and (2) as follows:

$$\text{Drug loading} = \text{Weight of loaded CUR} / \text{Weight of QCT NPs} \quad (1)$$

$$\text{Loading efficiency} = (\text{Weight of loaded CUR} / \text{Theoretical weight of CUR}) \times 100\% \quad (2)$$

XPS analysis

XPS was employed to verify successful PEGylation of CUR-loaded and drug-free QCT NPs. NP samples were drop-casted onto pre-cleaned[24] gold-coated silicon wafers (Micro to Nano V.O.F., Haarlem, Netherlands) and left to dry overnight. XPS measurements were carried out using a Thermo Fisher Scientific K-Alpha spectrometer utilizing a 72 W monochromated Al Kα x-ray source (with photon energy of 1,486 eV). The beam was focused to a spot size of 400 microns diameter on the sample surface, defining the analysis area, and three spots were scanned per sample. A dual beam flood gun was used to compensate for sample charging. Elemental composition was obtained from high-resolution spectra of the C 1s, O 1s, and S 2p regions. The C 1s peak was set to 285 eV for charge correction. Data analysis and peak deconvolution was conducted using CasaXPS.

In vitro release of CUR from CUR-loaded NPs

One milliliter of freshly prepared PEGylated CUR-loaded NPs (QCT@CUR@PEG NPs) was placed in a dialysis membrane (12 – 14 kD MWCO) and then immersed in 30 mL PBS (pH 7.4) containing 0.5% Tween 20 in a 60 mL glass vial. The vial was incubated at 100 rpm and 37 °C in a shaking water bath (GFL 1083, Burgwedel, Germany). At predetermined time points, 10 mL samples were withdrawn from the release medium and replaced with an equal volume of fresh medium to maintain sink conditions. The amount of CUR released was determined by measuring fluorescence of the samples at 460/40 nm excitation and 528/20 nm emission using a Biotek FLx800 fluorescence microplate reader (Winooski, VT, USA). Results were expressed as cumulative % amount of CUR released vs. time. The experiment was performed in triplicate.

Cell culture

CT26 murine colon carcinoma cells (ATCC, Manassas, VA, USA) were used as a model cell line in this study. Cells grown in RPMI 1640 medium (Invitrogen, Carlsbad, CA, USA) supplemented with 10% fetal calf serum, 1% L-glutamine, 100 U/mL penicillin, and 100 μg/mL streptomycin (Invitrogen) at 37 °C in 5% CO_2, and passaged twice a week.

Cytotoxicity assays

Cells were seeded in 96-well plates at a density of 1×10^4 cells per well (n = 4). After 24 h, cells were treated with free CUR (from a 54 mM stock solution in DMSO) or freshly prepared aqueous dispersions of CUR-loaded NPs (QCT@CUR_0.25 and QCT@CUR@PEG NPs; 10 mM) at concentrations spanning 1 – 1,000 μM CUR in complete media for 72 h. Note that the DMSO concentration in cells treated with free CUR did not exceed 2%, and that CUR concentration in the NPs was normalized by measuring drug loading in freshly prepared NPs as depicted in Equation 1. Cells were also incubated with drug-free QCT NPs and PEGylated QCT NPs (QCT@PEG NPs) at 1 – 1,000 μg/mL. After 72 h incubation, media was removed, cells were treated with the MTT reagent (0.5 mg/mL in complete RPMI 1640), and then incubated for an additional 3 h. Then, the media was carefully removed, and the formazan crystals were dissolved in 100 μL DMSO. The absorbance was read at 570 nm using a microplate reader (FLUOstar Optima, BMG Labtech, Ortenberg, Germany). Cell viability was expressed as % cell viability relative to cells incubated with complete media only. IC_{50} was calculated by fitting the data into a dose-response curve using Graphpad Prism 6.0e.

Cellular uptake studies

Cellular uptake was evaluated in CT26 cells by confocal laser scanning microscopy (CLSM) and flow cytometry. For confocal microscopy, cells (1×10^5 cells per well) were seeded in 4-well chamber slides (Nunc Lab-Tek, Thermo Scientific, Rochester, NY, USA) in complete media for 24 h. After, cells were incubated with free CUR or freshly prepared CUR-loaded QCT NPs (QCT@CUR_0.25 and QCT@CUR@PEG NPs) at concentrations equivalent to 20 μM CUR in complete media for 24 h. At the end of the incubation period, cells were washed three times with PBS and then fixed in 4% paraformaldehyde for 10 min. The fixed cells were then washed, mounted with ProLong™ Diamond antifade mountant containing DAPI (Invitrogen), and coverslipped. Imaging was performed using an LSM 780 microscope (Carl Zeiss GmbH, Gena, Germany). DAPI and CUR were excited using the 405 and 488 nm lines of a diode laser, respectively. Emission was filtered between 441 – 495 nm and 495 – 590 nm for DAPI and CUR, respectively. Images were captured using a Plan-Apochromat 20×/0.8 M27 objective.

For flow cytometry analysis, cells (1×10^5 cells per well) were seeded in 24-well plates overnight, and then treated with CUR or CUR-loaded QCT NPs (QCT@CUR_0.25 and QCT@CUR@PEG NPs) at concentrations equivalent to 20 μM CUR in complete media for 24 h. After 24 h, cells were washed, trypsinized, centrifuged, and resuspended in 250 μL PBS. Cell-associated fluorescence of CUR was quantified using the FL2 channel detector on a BD FACSCalibur flow cytometer (BD Biosciences, San Jose, CA, USA) from at least 10,000 gated cells per sample. The measurements were performed in triplicate.

Organ biodistribution studies by in vivo imaging

All animal experiments were performed in compliance with the UK Home Office (1989) Code of Practice for the housing and care of Animals used in Scientific Procedures. Mice (4-6-week-old

female Balb/c weighing ~20 g, Envigo, UK) were inoculated subcutaneously with 1×10^6 CT26 cells suspended in 0.1 mL PBS at the lower right flank. Mice (n = 3) received tail vein injections of DiR-labeled PEGylated QCT NPs (DiR-NP) diluted in PBS pH 7.4 at a DiR dose of 18.75 μg/kg. Imaging was performed at 1, 4, and 24 h post-injection using an IVIS Lumina Series III In Vivo Imaging System (Caliper Life Sciences, Perkin Elmer, USA). After 24 h, animals were euthanized and major organs (spleen, liver, lung, kidney, intestine, heart, and brain) as well as the tumors were excised for ex vivo imaging. Fluorescence images were obtained using the DiR filter as previously described.[39] The collected fluorescence emission signals were stored in efficiency units.

Tumor uptake of CUR-loaded NPs

To quantify tumor uptake of CUR-loaded NPs, female Balb/c mice (n = 3) bearing CT26 tumors were injected via tail vein with PEGylated CUR-loaded QCT NPs (QCT@CUR@PEG NPs) dispersed in 200 μL PBS pH 7.4 at a dose equivalent to 6 mg CUR/kg. At 30 h post-injection, animals were sacrificed and tumors were excised. Tumors were placed in a 6-well plate containing 2 mL serum-free RPMI 1640 and cut into small pieces using a scalpel. Two milliliters of serum-free medium was added to each well and the chopped pieces were transferred to universal test tubes. Digestion enzymes (collagenase type IV and DNase I; Thermo Fisher Scientific) were added to each tube at a final concentration of 2 mg/mL and 150 μg/mL for collagenase type IV and DNase I, respectively. Tumor pieces were then incubated for 45 min at 37 °C in a shaking water bath, vortexing every 15 min for 30 sec. After, 10 mL of 1% FBS in PBS was added to each tube, and the digested tissues were filtered using a 70 μm cell strainer in order to obtain uniform cell suspensions. The filtered suspensions were each centrifuged at 500 × g for 5 min at 4 °C, the

supernatants were discarded, and the pellets were resuspended in 10 mL PBS. Samples were centrifuged again at 500 × g for 5 min at 4 °C, the supernatants were discarded and cell pellets were resuspended in 1X ACK lysing buffer (Thermo Fisher Scientific) for 5 min, followed by adding 25 mL PBS to each sample. Cell suspensions were centrifuged again at 500 × g for 5 min at 4 °C, and the pellets were resuspended in 200 μL PBS for flow cytometry analysis as described above. Tumor homogenates of untreated animals were used as control.

Statistical analysis

Statistical analysis was performed in Graphpad Prism 6.0e using one-way analysis of variance (ANOVA) followed by Tukey's multiple comparisons test at a significance level of $p < 0.05$.

Results

Synthesis and characterization of CUR-loaded PEGylated QCT NPs

An overview of the one-pot QCT NP synthesis procedure and a proposed mechanism for NP formation is presented in Figure 1. We have previously demonstrated that QCT undergoes oxidative coupling in basic aqueous conditions yielding oligomers of ~5 monomers that are further stabilized by noncovalent interactions to form spherical colloidal aggregates.[24] In this study, TEA was used to catalyze QCT polymerization in DMSO by deprotonating the *o*-dihydroxyl groups on ring B, making the ring susceptible to nucleophilic addition reactions and leading to the formation of QCT oligomers. NP formation from QCT oligomers was then induced by solvent exchange in a process similar to self-assembly of amphiphilic copolymers.

As shown in Table 2, QCT alone (QCT NPs) formed NPs around 33 nm in size, similar to our previous findings.[24] The FT-IR spectrum of QCT (Figure S1) showed several characteristic bands corresponding to O-H (3000 – 3600 cm^{-1}), C=O (1600 – 1700 cm^{-1}), and C=C aromatic stretching (1500 – 1600 cm^{-1}), as well as and O-H bending (1300 – 1400 cm^{-1}). QCT NPs exhibited similar bands, which indicates that QCT oxidation and polymerization did not lead to the formation of new functional groups.

NaOMe, $AlCl_3$, and $AlCl_3$/HCl were used as UV shift reagents to determine the presence of free –OH groups in QCT NPs, specifically the *o*-dihydroxyl groups on ring B, since the oxidative coupling reactions behind QCT NP formation relied on oxidation of these groups into quinones (Figure 1B). As depicted in Figure S2, the characteristic absorption bands of QCT appeared at 371 nm (band I) and 256 nm (band II). After adding NaOMe, band I was shifted to 422 nm, which indicates a free –OH group at C-3. The presence of a free –OH group at C-7 was confirmed by the appearance of a new peak at 327 nm. The addition of $AlCl_3$/HCl caused a shift

in band I to 428 nm, verifying the presence of –OH groups on C-3 and C-5. Upon the addition of $AlCl_3$, band I was shifted to 457 nm, which was 29 nm greater than the shift observed with $AlCl_3$/HCl, supporting the presence of *o*-dihydroxyl groups on ring B (Figure S2). As for QCT NPs, band II appeared at 257 nm while band I was shifted to 348 nm (Figure S2). The presence of a free –OH group at C-3 was confirmed upon the addition of NaOMe, where band I was shifted to 476 nm. A new peak also appeared at 390 nm, which is attributed to the presence of a free –OH group at C-7. After adding $AlCl_3$, band I was shifted to 445 nm, confirming the presence of –OH groups on C-3 and C-5. The addition of HCl did not affect this shift, which signifies the absence of *o*-dihydroxyl groups on ring B, most likely since they have been oxidized to quinones, becoming unavailable to react with $AlCl_3$ (Figure S2). This supports the proposed NP synthesis mechanism depicted in Figure 1B.

PEGylated NPs were obtained by adding mPEG-SH to the reaction in DMSO by exploiting the fact that the oxidized catechols on ring B of QCT are susceptible to nucleophilic addition reactions (Figure 1B), facilitating the incorporation of amine- or thiol-terminated ligands. Upon incorporation of mPEG-SH, particle size of PEGylated QCT NPs (QCT@PEG NPs) was increased to 166 nm. This is consistent with previous reports, where surface PEGylation of polyphenol NPs led to an increase in the hydrodynamic diameter depending on the conformation of the PEG chains.[20, 40] Given the notable size increase of QCT@PEG NPs compared to QCT NPs (from 33 to 166 nm), it is probable that part of the PEG chain became incorporated in the NP core. The FT-IR spectrum of QCT@PEG NPs (Figure S1) exhibited C-H and C-O-C stretching bands between 2700 – 3000 cm^{-1} and 1000 – 1200 cm^{-1}, respectively, attributed to the presence of PEG.

The ability of the NPs to incorporate CUR with or without surface PEGylation was investigated by adding CUR at different molar ratios relative to QCT. As depicted in Table 2,

CUR-loaded QCT NPs prepared at QCT: CUR ratios of 1:1, 1:0.5, and 1:0.1 (QCT@CUR_1, QCT@CUR_0.5, and QCT@CUR_0.1, respectively) were in the size range 76 – 97 nm and had polydispersity indices (PDI) ranging from 0.22 – 0.38. Drug loading efficiency was lowest for QCT@CUR_1 and QCT@CUR_0.5 NPs (4.7 and 9.9%, respectively). QCT@CUR_0.25 NPs with a QCT: CUR ratio of 1:0.25 exhibited the smallest PDI (0.05), and the highest loading efficiency (91.0%), indicating that an optimum loading capacity was reached. The significant size increase observed in QCT@CUR_0.25 NPs (140 nm) was likely attributed to the greater amount of CUR incorporated compared to the other formulations. Having obtained NPs with the narrowest size distribution and the highest loading capacity with QCT@CUR_0.25 NPs, a QCT: CUR ratio of 1:0.25 was chosen for the synthesis of PEGylated CUR-loaded QCT NPs (QCT@CUR@PEG NPs). The NPs exhibited a spherical morphology (Figure 2), a mean hydrodynamic diameter of 90 nm, a relatively narrow size distribution with a PDI of 0.12, and a loading efficiency of 51.1% (Table 2). The lower loading efficiency of QCT@CUR@PEG NPs compared to their nonPEGylated counterparts is likely attributed to steric hindrance by the PEG chains which interfered with CUR loading. The decrease in drug loading capacity in turn resulted in NPs with smaller diameter. CUR loading did not result in any spectral changes as observed by UV-Vis (Figure S3), which signifies that CUR is only physically entrapped within the NPs.

Zeta potential measurements were conducted in order to confirm successful incorporation of PEG on the NP surface, as PEG is a neutral polymer whereas QCT carries a partially negative surface charge due to the presence of electron-rich aromatic rings. As observed in Table 2, all NPs displayed partially negative zeta potential values ranging from -11.3 to -21.7 mV, as previously reported for QCT NPs.[24] However, the PEGylated formulations, QCT@PEG and QCT@CUR@PEG NPs, displayed significantly lower surface charge values ($p < 0.001$ and $p <$

0.0001, respectively) compared to their nonPEGylated counterparts, QCT and QCT@CUR_0.25 NPs (Figure 3A). These findings strongly indicate partial shielding of the negative surface charge of QCT by the PEG corona.

NP PEGylation was further verified by XPS to obtain the surface elemental composition of the synthesized NPs. PEGylated NPs (QCT@PEG and QCT@CUR@PEG NPs) showed a significant increase in S 2p signals at a binding energy of ~163 eV, attributed to the presence of thiol groups of mPEG-SH (Figure 3C). Moreover, PEGylated NPs were associated with a significantly lower C/O ratio (Figure 3D) and an increase in C-O-C components (Figure S4 and Figure S5), consistent with XPS measurements of PEGylated NPs.[17, 20, 24] These findings combined with surface charge measurements corroborate our hypothesis that the one-pot procedure can successfully yield surface-functionalized QCT NPs.

In vitro release of CUR from CUR-loaded NPs

CUR release from QCT@CUR@PEG NPs was investigated in PBS at pH 7.4. As shown in Figure 4, drug release was sustained throughout the duration of the study, with 50.9% of CUR released within the first 4 h, 95.0% released after 24 h, and 99.1% released after 4 days. Interestingly, we observed slower release with the prototype QCT NPs encapsulating DOX, where only 47.1% of DOX was released within 24 h and 70.7% released after 4 days.[24] The marked difference in release kinetics suggest a weaker interaction between CUR and QCT compared to DOX, which facilitated drug release.

Cytotoxicity of CUR-loaded NPs in CT26 cells

Cytotoxicity assays were conducted in order to verify whether the NP synthesis method compromised CUR's pharmacologic activity. CT26 cells were treated with increasing

concentrations of CUR alone or loaded in QCT NPs (QCT@CUR_0.25 and QCT@CUR@PEG NPs) up to 72 h. Drug-free NPs (QCT NPs and QCT@PEG NPs) exhibited low toxicity up to 1 mg/mL (Figure S6). As shown in Figure 5, CUR exhibited dose-dependent cytotoxicity with an IC_{50} of 28.5 μM, which was close to literature values.[39] PEGylated CUR-loaded NPs (QCT@CUR@PEG NPs) were associated with a similar potency at an IC_{50} of 34.7 μM. Conversely, nonPEGylated NPs (QCT@CUR_0.25 NPs) showed a reduction in potency with an IC_{50} of 128.3 μM. The difference may be attributed to the greater steric stability of QCT@CUR@PEG NPs in the cell culture medium imparted by the surface-exposed PEG chains. The nonPEGylated NPs were more prone to aggregation, which likely hindered their cellular uptake. Although the new NP formulation of CUR did not significantly enhance its cytotoxicity, the NPs were completely soluble in water unlike free CUR, which needed to be solubilized in DMSO for the in vitro experiments.

Cellular uptake of CUR-loaded NPs by confocal microscopy and flow cytometry

Intracellular uptake of CUR alone or loaded in QCT NPs (QCT@CUR_0.25 and QCT@CUR@PEG NPs) was visualized by confocal microscopy, enabled by the intrinsic fluorescence of CUR. CT26 cells were incubated with 20 μM CUR or an equivalent concentration in QCT NPs for 24 h. As observed in Figure 6A, stronger green fluorescence signals were obtained from cells treated with free CUR and QCT@CUR@PEG NPs compared to those treated with QCT@CUR_0.25 NPs. The results were consistent with the cytotoxicity experiments, were QCT@CUR_0.25 NPs exhibited the lowest potency compared to QCT@CUR@PEG NPs and the free drug, which further confirms reduced cellular uptake of the nonPEGylated NPs due to their lower stability in the culture medium. Cellular internalization was also measured by flow

cytometry, by quantifying cell-associated mean fluorescence intensities (MFI) (Figure 6B and Figure 6C). Free CUR and QCT@CUR@PEG NPs showed similar MFI values, which were both significantly higher than those associated with QCT@CUR_0.25 NPs, in line with confocal microscopy observations. Taken together, the cytotoxicity and cellular uptake experiments provided strong evidence on the successful synthesis of functional NPs that are readily internalized by the cells with demonstrated in vitro anti-cancer activity.

In vivo biodistribution and tumor uptake of systemically-administered NPs

Having shown promising bioactivity in vitro, in vivo biodistribution studies were carried out on PEGylated NPs in CT26 tumor-bearing mice. NPs were loaded with DiR to enable whole body imaging throughout the study, and ex vivo imaging of excised major organs afterwards. Representative dorsal view images of control and NP-treated animals are shown in Figure 7A, while images of excised organs and their corresponding fluorescence intensities (expressed as total radiant efficiency per g organ) are depicted in Figure 7B and Figure 7C, respectively. Tumor accumulation of DiR-labeled NPs can be clearly observed over the time course of the study, as indicated by the steady increase in fluorescence signal intensities at the tumor sites from 1 h up to 24 h. Excised tumors showed fluorescence intensities that were significantly higher than the background signals, indicating some degree of tumor accumulation (Figure 7C). We also observed NP accumulation in the spleen and lung, which may be attributed to NP uptake by phagocytes and macrophages of the reticuloendothelial system. Since whole body images showed strong fluorescence signals around the tumors, while tumor accumulation was lower than expected, tumor excision for CUR NP-treated animals was performed at 30 h post-injection, to enable more tumor uptake to take place. Flow cytometry analysis of tumor homogenates after the administration of

QCT@CUR@PEG NPs at a CUR dose of 6 mg/kg showed significantly higher MFI compared to PBS-treated controls (Figure 8), indicating tumor uptake of the NPs following systemic administration.

Discussion

Oxidative self-polymerization of polyphenols has attracted great interest over the past decade, and has mainly been applied to produce versatile multifunctional coatings on a variety of substrates.[11, 13] It has also inspired the development of untemplated standalone NPs from coating precursors such as dopamine, tannic acid, green tea polyphenols, and most recently, QCT. Polyphenol NPs have been synthesized through a variety of approaches, all of which have relied on oxidation-triggered polymerization of the polyphenol precursor. This may be achieved in aqueous alkaline solutions[19-20, 24, 40-42] or using an oxidizing agent such as hydrogen peroxide,[43] sodium metaperiodate,[44] or copper sulfate,[21, 23] with or without the aid of a chelating agent such as ferric chloride.[45] The reactive nature of these NPs was exploited to functionalize them with surface ligands, drug molecules, or imaging agents through sequential incubation with the molecule of interest, followed by additional purification steps. We present in this work a straightforward greener approach to polyphenol NP synthesis where NP formation, hydrophobic drug loading, and surface functionalization can be achieved in one step. The new procedure was carried out at ambient conditions and cut down on reaction time and energy consumption.

UV-Vis analysis revealed that the catechol groups of the second generation QCT NPs were oxidized to quinones, similar to what we observed in the prototype NPs, suggesting that they were formed via a similar mechanism, i.e. oxidative self-polymerization (Figure 1B). TEA triggered the deprotonation/oxidation of *o*-dihydroxyl groups on ring B of QCT, leading to the formation of reactive quinones. This was likely followed by a series of coupling reactions that resulted in the formation of QCT oligomers. Solvent exchange with water via dialysis allowed these oligomers to self-assemble into larger nanoscale aggregates brought together by non-covalent interactions. Polyphenol polymerization in nonaqueous media has only been reported for dopamine, where various substrates

were coated with polydopamine in organic protic solvents (ethanol or methanol) containing piperidine to deprotonate the catechol moieties and various ligands for simultaneous functionalization.[46] In the present work, we demonstrate that polyphenol polymerization can also be achieved in DMSO, an aprotic universal solvent, which holds great promise for translating the procedure to water insoluble polyphenol NP precursors and cargo.

When we tested the ability of the NPs to incorporate CUR, an optimum drug loading capacity and NP polydispersity were achieved at a QCT: CUR molar ratio of 1:0.25, which produced the largest size NPs. Interestingly, when the same QCT: CUR ratio was used to synthesize PEGylated NPs, it resulted in a smaller hydrodynamic diameter and a lower drug loading capacity. These observations may be attributed to steric hindrance imparted by the PEG chains, which likely interfered with CUR loading, resulting in smaller size NPs.

We investigated the viability of the one-pot procedure to produce surface-functionalized NPs by FT-IR, DLS, and XPS measurements, all of which verified the presence of surface-immobilized PEG. PEGylation was also confirmed indirectly by observing enhanced cellular uptake and cytotoxicity of PEGylated CUR-loaded NPs (QCT@CUR@PEG NPs) compared to nonPEGylated NPs (QCT@CUR_0.25 NPs), which was likely due to the steric stability enabled by the PEG corona in serum-containing media.

In vitro release of CUR was conducted under physiologically relevant conditions, achieving sustained release of the drug over several days. The release kinetics observed in this study were faster than those obtained with the first generation DOX-loaded QCT NPs, where NPs were sequentially PEGylated and loaded with the drug. Relatively fast CUR release suggests that it is less strongly bound to the QCT core. This may in part be attributed to crowding by the PEG chain entrapped within the NP, as indicated by the marked increase in PEGylated NP size

compared to unmodified QCT NPs and reduced drug loading compared to QCT@CUR_0.25 NPs. Our findings also indicate that the PEGylation and drug incorporation method (one-pot versus multistep approach) may be exploited to tune drug release kinetics.

CUR released from the NPs maintained its bioactivity, which was demonstrated by the comparable potency between QCT@CUR@PEG NPs and free CUR against CT26 cells. The NPs were efficiently taken up by the cells within 24 h as confirmed by confocal microscopy and flow cytometry. The promising in vitro performance of the NPs led us to investigate their biodistribution in vivo. PEGylated DiR-labeled QCT NPs were injected into CT26 tumor-bearing mice, and in vivo imaging up to 24 h revealed their gradual tumor accumulation. Ex vivo imaging of excised tumors showed detectable fluorescence signals, with higher NP accumulation observed in the spleen and lung compared to the tumors. Given that in vivo imaging results showed steady accumulation of the NPs at the tumor site, we postulated that the NPs were still in the tumor vasculature at 24 h post-injection, and that more time was needed for tumor uptake to take place. Thus, when tumor-bearing animals were injected with CUR-loaded NPs up to 30 h, measurable amounts of CUR were detected by flow cytometry analysis of excised tumor homogenates. Bearing in mind the heterogeneous nature of tumor tissues and the less reliable EPR effect, it is evident that the synthesized NPs would greatly benefit from an active targeting mechanism. The versatile nature of QCT NPs is expected to allow the convenient fabrication of active targeted NPs to achieve more selective tumor accumulation and minimize off-target uptake. Taken together, these preliminary findings revealed valuable information about the in vivo fate of QCT NPs as a promising cancer-targeted delivery platform.

Conclusion

In this work, we tested the hypothesis that a functional anti-cancer nanomedicine can be synthesized from the abundant plant polyphenol QCT in a green one-pot procedure. PEGylated CUR-loaded NPs were synthesized by base-catalyzed oxidative self-polymerization of QCT in DMSO, a universal organic solvent, making the oxidized catechol moieties of QCT reactive toward a nucleophilic ligand such as thiol-terminated PEG. The NPs were formed upon gradual addition of water, entrapping CUR in the core. Characterization of the NPs by various techniques confirmed our hypothesis. Bioassays in a murine colon cancer model revealed the potent cytotoxicity and efficient cellular uptake of CUR-loaded NPs. In vivo biodistribution studies demonstrated the NPs' passive targeting potential and shed important insights into their in vivo fate. The unique features of these NPs make them promising candidates as versatile nanocarriers with the ability to incorporate hydrophobic drug molecules and surface ligands in a simple procedure with minimal equipment.

Supporting Information

The Supporting Information is available free of charge on the ACS Publications website at http://pubs.acs.org.

FT-IR, UV-Vis, and XPS spectra, and results from cell viability assays (PDF).

Conflicts of interest

There are no conflicts to declare.

Acknowledgments

This work was supported by Al-Zaytoonah University of Jordan (Grant no. 15/28/2017-2018); PhosAgro/UNESCO/IUPAC Partnership in Green Chemistry for Life (Contract no. 4500378258); TWAS-COMSTECH (Grant no. 17-134 RG/MSN/AF/AC_C-FR3240300066); and the Academy of Medical Sciences (2018 Daniel Turnberg Travel Fellowship). XPS data collection was performed at the EPSRC National Facility for XPS ('HarwellXPS') under contract no. PR16195. The authors would like to thank Rula Baqain and Aya Abusheikha from the Cell Therapy Center, Amman, Jordan for assistance with electron microscopy and confocal microscopy imaging.

References

(1) WHO Cancer Fact Sheet. http://www.who.int/mediacentre/factsheets/fs297/en/ (accessed Dec 29).

(2) Popovic, Z.; Liu, W. H.; Chauhan, V. P.; Lee, J.; Wong, C.; Greytak, A. B.; Insin, N.; Nocera, D. G.; Fukumura, D.; Jain, R. K.; Bawendi, M. G., A Nanoparticle size series for in vivo fluorescence imaging. *Angew. Chem.-Int. Edit.* **2010,** *49* (46), 8649-8652, DOI: 10.1002/anie.201003142.

(3) Ulbrich, K.; Hola, K.; Subr, V.; Bakandritsos, A.; Tucek, J.; Zboril, R., Targeted drug delivery with polymers and magnetic nanoparticles: Covalent and noncovalent approaches, release control, and clinical studies. *Chemical Rev.* **2016,** *116* (9), 5338-5431, DOI: 10.1021/acs.chemrev.5b00589.

(4) Sunoqrot, S.; Hamed, R.; Abdel-Halim, H.; Tarawneh, O., Synergistic interplay of medicinal chemistry and formulation strategies in nanotechnology – From drug discovery to nanocarrier design and development. *Curr. Topic. Med. Chem.* **2017,** *17* (13), 1451-1468, DOI: 10.2174/1568026616666161222111656.

(5) Nicolas, J.; Mura, S.; Brambilla, D.; Mackiewicz, N.; Couvreur, P., Design, functionalization strategies and biomedical applications of targeted biodegradable/biocompatible polymer-based nanocarriers for drug delivery. *Chem. Soc. Rev.* **2013,** *42* (3), 1147-1235, DOI: 10.1039/c2cs35265f.

(6) Torchilin, V. P., Multifunctional, stimuli-sensitive nanoparticulate systems for drug delivery. *Nat. Rev. Drug Discovery* **2014,** *13* (11), 813-827, DOI: 10.1038/nrd4333.

(7) El-Gogary, R. I.; Rubio, N.; Wang, J. T.-W.; Al-Jamal, W. T.; Bourgognon, M.; Kafa, H.; Naeem, M.; Klippstein, R.; Abbate, V.; Leroux, F., Polyethylene glycol conjugated polymeric nanocapsules for targeted delivery of quercetin to folate-expressing cancer cells in vitro and in vivo. *ACS Nano* **2014,** *8* (2), 1384-1401, DOI: 10.1021/nn405155b.

(8) Quadir, M. A.; Morton, S. W.; Mensah, L. B.; Shopsowitz, K.; Dobbelaar, J.; Effenberger, N.; Hammond, P. T., Ligand-decorated click polypeptide derived nanoparticles for targeted drug delivery applications. *Nanomedicine* **2017,** *13* (5), 1797-1808, DOI: 10.1016/j.nano.2017.02.010.

(9) Zhou, Z.; Badkas, A.; Stevenson, M.; Lee, J.-Y.; Leung, Y.-K., Herceptin conjugated PLGA-PHis-PEG pH sensitive nanoparticles for targeted and controlled drug delivery. *Int. J. Pharm.* **2015,** *487* (1), 81-90, DOI: 10.1016/j.ijpharm.2015.03.081.

(10) Banerjee, A.; Qi, J.; Gogoi, R.; Wong, J.; Mitragotri, S., Role of nanoparticle size, shape and surface chemistry in oral drug delivery. *J. Controlled Release* **2016,** *238*, 176-185, DOI: 10.1016/j.jconrel.2016.07.051.

(11) Lee, H. A.; Ma, Y.; Zhou, F.; Hong, S.; Lee, H., Material-independent surface chemistry beyond polydopamine coating. *Acc. Chem. Res.* **2019,** *52* (3), 704-713, DOI: 10.1021/acs.accounts.8b00583.

(12) Quideau, S.; Deffieux, D.; Douat-Casassus, C.; Pouységu, L., Plant polyphenols: Chemical properties, biological activities, and synthesis. *Angew. Chem.-Int. Edit.* **2011,** *50* (3), 586-621, DOI: 10.1002/anie.201000044.

(13) Ye, Q.; Zhou, F.; Liu, W. M., Bioinspired catecholic chemistry for surface modification. *Chem. Soc. Rev.* **2011,** *40* (7), 4244-4258, DOI: 10.1039/c1cs15026j.

(14) Lee, H.; Dellatore, S. M.; Miller, W. M.; Messersmith, P. B., Mussel-inspired surface chemistry for multifunctional coatings. *Science* **2007,** *318* (5849), 426-430, DOI: 10.1126/science.1147241.
(15) Lee, H.; Rho, J.; Messersmith, P. B., Facile conjugation of biomolecules onto surfaces via mussel adhesive protein inspired coatings. *Adv. Mater.* **2009,** *21* (4), 431-434, DOI: 10.1002/adma.200801222.
(16) Li, J.; Wu, S. X.; Wu, C. C.; Qiu, L. P.; Zhu, G. Z.; Cui, C.; Liu, Y.; Hou, W. J.; Wang, Y. Y.; Zhang, L. Q.; Teng, I. T.; Yang, H. H.; Tan, W. H., Versatile surface engineering of porous nanomaterials with bioinspired polyphenol coatings for targeted and controlled drug delivery. *Nanoscale* **2016,** *8* (16), 8600-8606, DOI: 10.1039/c6nr00600k.
(17) Abouelmagd, S. A.; Meng, F. F.; Kim, B. K.; Hyun, H.; Yeo, Y., Tannic acid-mediated surface functionalization of polymeric nanoparticles. *ACS Biomater. Sci. Eng.* **2016,** *2* (12), 2294-2303, DOI: 10.1021/acsbiomaterials.6b00497.
(18) Liu, Y.; Ai, K.; Liu, J.; Deng, M.; He, Y.; Lu, L., Dopamine-melanin colloidal nanospheres: An efficient near-infrared photothermal therapeutic agent for in vivo cancer therapy. *Adv. Mater.* **2013,** *25* (9), 1353-1359, DOI: 10.1002/adma.201204683.
(19) Ju, K.-Y.; Lee, Y.; Lee, S.; Park, S. B.; Lee, J.-K., Bioinspired polymerization of dopamine to generate melanin-like nanoparticles having an excellent free-radical-scavenging property. *Biomacromolecules* **2011,** *12* (3), 625-632, DOI: 10.1021/bm101281b.
(20) Amin, D. R.; Sugnaux, C.; Lau, K. H. A.; Messersmith, P. B., Size control and fluorescence labeling of polydopamine melanin-mimetic nanoparticles for intracellular imaging. *Biomimetics* **2017,** *2* (3), 17, DOI: 10.3390/biomimetics2030017.
(21) Chen, Z.; Wang, C.; Chen, J.; Li, X., Biocompatible, functional spheres based on oxidative coupling assembly of green tea polyphenols. *J. Am. Chem. Soc.* **2013,** *135* (11), 4179-4182, DOI: 10.1021/ja311374b.
(22) Markova, Z.; Novak, P.; Kaslik, J.; Plachtova, P.; Brazdova, M.; Jancula, D.; Siskova, K. M.; Machala, L.; Marsalek, B.; Zboril, R., Iron (II, III)–polyphenol complex nanoparticles derived from green tea with remarkable ecotoxicological impact. *ACS Sustainable Chem. Eng.* **2014,** *2* (7), 1674-1680, DOI: 10.1021/sc5001435.
(23) Xiang, S.; Yang, P.; Guo, H.; Zhang, S.; Zhang, X.; Zhu, F.; Li, Y., Green tea makes polyphenol nanoparticles with radical-scavenging activities. *Macromol. Rapid Commun.* **2017,** *38* (23), 1700446, DOI: 10.1002/marc.201700446.
(24) Sunoqrot, S.; Al-Shalabi, E.; Messersmith, P. B., Facile synthesis and surface modification of bioinspired nanoparticles from quercetin for drug delivery. *Biomater. Sci.* **2018,** *6* (10), 2656-2666, DOI: 10.1039/C8BM00587G.
(25) Zeng, X.; Liu, G.; Tao, W.; Ma, Y.; Zhang, X.; He, F.; Pan, J.; Mei, L.; Pan, G., A drug-self-gated mesoporous antitumor nanoplatform based on pH-sensitive dynamic covalent bond. *Adv. Funct. Mater.* **2017,** *27* (11), 1605985, DOI: 10.1002/adfm.201605985.
(26) Zeng, X.; Luo, M.; Liu, G.; Wang, X.; Tao, W.; Lin, Y.; Ji, X.; Nie, L.; Mei, L., Polydopamine-modified black phosphorous nanocapsule with enhanced stability and photothermal performance for tumor multimodal treatments. *Adv. Sci.* **2018,** *5* (10), 1800510, DOI: 10.1002/advs.201800510.
(27) Liu, S.; Pan, J.; Liu, J.; Ma, Y.; Qiu, F.; Mei, L.; Zeng, X.; Pan, G., Dynamically PEGylated and borate-coordination-polymer-coated polydopamine nanoparticles for synergetic tumor-targeted, chemo-photothermal combination therapy. *Small* **2018,** *14* (13), 1703968, DOI: 10.1002/smll.201703968.

(28) Cheng, W.; Nie, J.; Gao, N.; Liu, G.; Tao, W.; Xiao, X.; Jiang, L.; Liu, Z.; Zeng, X.; Mei, L., A Multifunctional nanoplatform against multidrug resistant cancer: Merging the best of targeted chemo/gene/photothermal therapy. *Adv. Funct. Mater.* **2017,** *27* (45), 1704135, DOI: 10.1002/adfm.201704135.
(29) Priyadarsini, K., The chemistry of curcumin: From extraction to therapeutic agent. *Molecules* **2014,** *19* (12), 20091-20112, DOI: 10.3390/molecules191220091.
(30) Sun, M.; Su, X.; Ding, B.; He, X.; Liu, X.; Yu, A.; Lou, H.; Zhai, G., Advances in nanotechnology-based delivery systems for curcumin. *Nanomedicine* **2012,** *7* (7), 1085-1100, DOI: 10.2217/nnm.12.80.
(31) Prajakta, D.; Ratnesh, J.; Chandan, K.; Suresh, S.; Grace, S.; Meera, V.; Vandana, P., Curcumin loaded pH-sensitive nanoparticles for the treatment of colon cancer. *J. Biomed. Nanotechnol.* **2009,** *5* (5), 445-455, DOI: 10.1166/jbn.2009.1038.
(32) Xu, X.-Y.; Meng, X.; Li, S.; Gan, R.-Y.; Li, Y.; Li, H.-B., Bioactivity, health benefits, and related molecular mechanisms of curcumin: Current progress, challenges, and perspectives. *Nutrients* **2018,** *10* (10), 1553, DOI: 10.3390/nu10101553.
(33) Ji, W.-H.; Xiao, Z.-B.; Liu, G.-Y.; Zhang, X., Development and application of nano-flavor-drug carriers in neurodegenerative diseases. *Chin. Chem. Lett.* **2017,** *28* (9), 1829-1834, DOI: 10.1016/j.cclet.2017.06.024.
(34) Yang, Z.; Peng, Y.; Qiu, L., pH-Responsive supramolecular micelle based on host-guest interaction of poly(β-amino ester) derivatives and adamantyl-terminated poly(ethylene glycol) for cancer inhibition. *Chin. Chem. Lett.* **2018,** *29* (12), 1839-1844, DOI: 10.1016/j.cclet.2018.11.009.
(35) Zhang, T.; Chen, Y.; Ge, Y.; Hu, Y.; Li, M.; Jin, Y., Inhalation treatment of primary lung cancer using liposomal curcumin dry powder inhalers. *Acta Pharm. Sin. B* **2018,** *8* (3), 440-448, DOI: 10.1016/j.apsb.2018.03.004.
(36) Tao, J.; Chow, S. F.; Zheng, Y., Application of flash nanoprecipitation to fabricate poorly water-soluble drug nanoparticles. *Acta Pharm. Sin. B* **2018,** *9*(1), 4-8, DOI: 10.1016/j.apsb.2018.11.001.
(37) Markham, K. R.; Mabry, T. J., A procedure for the ultraviolet spectral detection of ortho-dihydroxyl groups in flavonoids. *Phytochemistry* **1968,** *7* (7), 1197-1200, DOI: 10.1016/S0031-9422(00)88270-9.
(38) Suh, H. J.; Lee, J. M.; Cho, J. S.; Kim, Y. S.; Chung, S. H., Radical scavenging compounds in onion skin. *Food Res. Int.* **1999,** *32* (10), 659-664, DOI: 10.1016/S0963-9969(99)00141-6.
(39) Klippstein, R.; Wang, J. T. W.; El-Gogary, R. I.; Bai, J.; Mustafa, F.; Rubio, N.; Bansal, S.; Al-Jamal, W. T.; Al-Jamal, K. T., Passively targeted curcumin-loaded PEGylated PLGA nanocapsules for colon cancer therapy in vivo. *Small* **2015,** *11* (36), 4704-4722, DOI: 10.1002/smll.201403799.
(40) Amin, D. R.; Higginson, C. J.; Korpusik, A. B.; Gonthier, A. R.; Messersmith, P. B., Untemplated resveratrol-mediated polydopamine nanocapsule formation. *ACS Appl. Mater. Interfaces* **2018,** *10* (40), 34792-34801, DOI: 10.1021/acsami.8b14128.
(41) Ho, C.-C.; Ding, S.-J., The pH-controlled nanoparticles size of polydopamine for anti-cancer drug delivery. *J. Mater. Sci.: Mater. Med.* **2013,** *24* (10), 2381-2390, DOI: 10.1007/s10856-013-4994-2.
(42) Yu, X.; Tang, X.; He, J.; Yi, X.; Xu, G.; Tian, L.; Zhou, R.; Zhang, C.; Yang, K., Polydopamine nanoparticle as a multifunctional nanocarrier for combined

radiophotodynamic therapy of cancer. *Part. Part. Syst. Charact.* **2017,** *34* (2), 1600296, DOI: 10.1002/ppsc.201600296.

(43) Zhang, X.; Wang, S.; Xu, L.; Feng, L.; Ji, Y.; Tao, L.; Li, S.; Wei, Y., Biocompatible polydopamine fluorescent organic nanoparticles: Facile preparation and cell imaging. *Nanoscale* **2012,** *4* (18), 5581-5584, DOI: 10.1039/C2NR31281F.

(44) El Yakhlifi, S.; Ihiawakrim, D.; Ersen, O.; Ball, V., Enzymatically active polydopamine @ alkaline phosphatase nanoparticles produced by $NaIO_4$ oxidation of dopamine. *Biomimetics* **2018,** *3* (4), 36-48, DOI: 10.3390/biomimetics3040036.

(45) Saowalak, K.; Titipun, T.; Somchai, T.; Chalermchai, P., Iron(III)-tannic molecular nanoparticles enhance autophagy effect and T1 MRI contrast in liver cell lines. *Sci. Rep.* **2018,** *8* (1), 6647, DOI: 10.1038/s41598-018-25108-1.

(46) You, I.; Jeon, H.; Lee, K.; Do, M.; Seo, Y. C.; Lee, H. A.; Lee, H., Polydopamine coating in organic solvent for material-independent immobilization of water-insoluble molecules and avoidance of substrate hydrolysis. *J. Ind. Eng. Chem.* **2017,** *46*, 379-385, DOI: 10.1016/j.jiec.2016.11.007.

Tables and Figures

Table 1. Summary of the different NPs synthesized in this study.

NP	QCT: CUR (mol/mol)	QCT (mg)	CUR (mg)
QCT	-	10.0	-
QCT@PEG[a]	-	10.0	-
QCT@CUR_1	1:1	10.0	12.2
0.5_CUR@QCT	1:0.5	10.0	6.1
0.25_CUR@QCT	1:0.25	10.0	3.0
0.1_CUR@QCT	1:0.1	10.0	1.2
QCT@CUR@PEG[a]	1:0.25	10.0	3.0

[a]PEGylated NPs were prepared by adding mPEG-SH (10 mM) to the reaction mixture.

Table 2. Characterization of the NPs synthesized in this study.

NP	Particle size (nm)	PDI[a]	Zeta potential (mV)	Loading (μg CUR/mg NP)	Loading efficiency (%)
QCT	33 ± 5	0.40 ± 0.01	-16.3 ± 1.1	-	-
QCT@PEG	166 ± 35	0.37 ± 0.09	-11.3 ± 1.2	-	-
QCT@CUR_1	76 ± 6	0.38 ± 0.03	-17.6 ± 1.6	5.8 ± 2.3	4.7 ± 1.9
0.5_CUR@QCT	69 ± 24	0.46 ± 0.05	-16.7 ± 1.2	6.0 ± 2.7	9.9 ± 4.8
0.25_CUR@QCT	140 ± 2	0.05 ± 0.03	-21.7 ± 0.8	27.7 ± 1.8	91.0 ± 6.0
0.1_CUR@QCT	97 ± 18	0.22 ± 0.02	-16.9 ± 0.8	6.3 ± 1.5	51.2 ± 13.5
QCT@CUR@PEG	90 ± 2	0.13 ± 0.01	-11.6 ± 1.0	15.5 ± 9.8	51.1 ± 6.5

[a]Polydispersity index

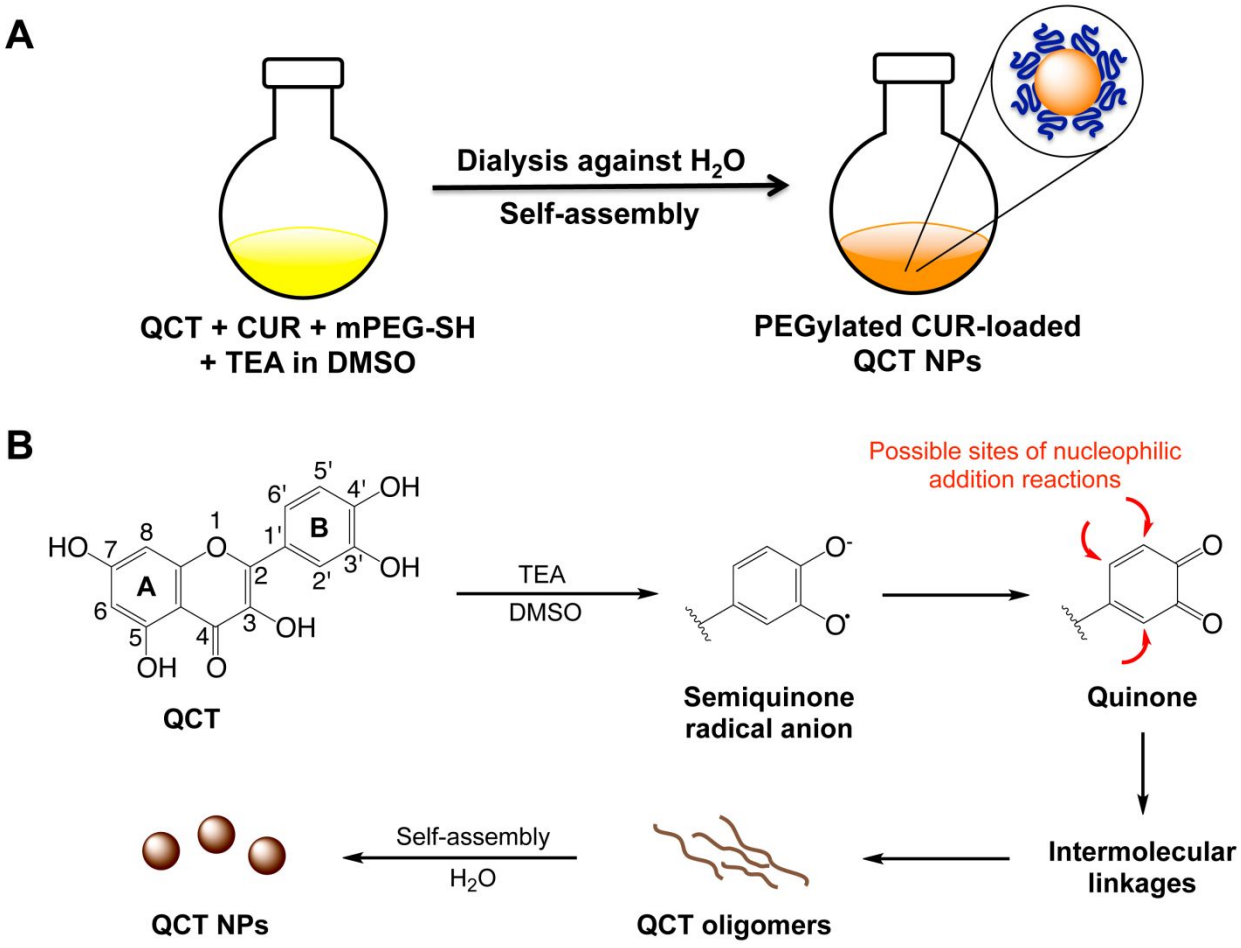

Figure 1. (A) One-pot synthesis of PEGylated CUR-loaded QCT NPs; (B) Proposed NP formation mechanism by base-catalyzed oxidative polymerization of QCT and subsequent self-assembly into NPs. (Reproduced with permission from ref. 24. Copyright The Royal Society of Chemistry).

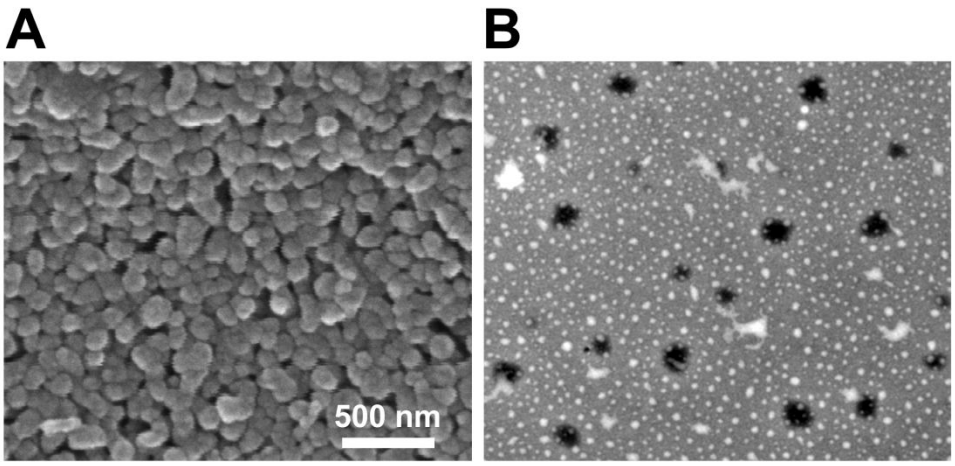

Figure 2. (A) SEM and (B) TEM images of PEGylated CUR-loaded NPs (QCT@CUR@PEG NPs) showing their spherical morphology.

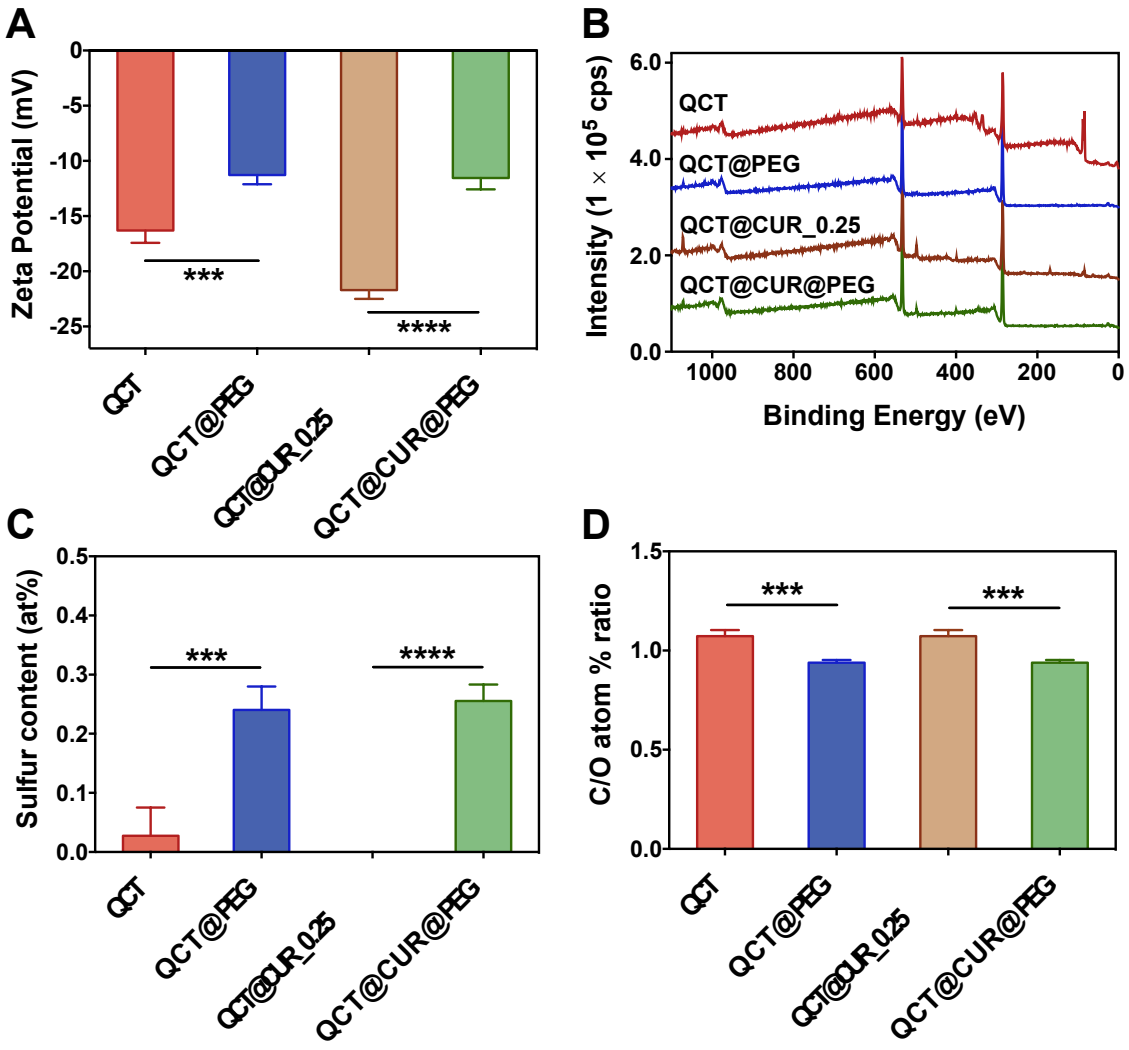

Figure 3. Confirmation of NP PEGylation by DLS and XPS. (A) Zeta potential of QCT NPs, PEGylated QCT NPs (QCT@PEG NPs), CUR-loaded QCT NPs (QCT@CUR_0.25 NPs) and PEGylated CUR-loaded QCT NPs (QCT@CUR@PEG NPs). A significant reduction in zeta potential was observed after PEGylation, which verifies successful surface modification of QCT@PEG and QCT@CUR@PEG NPs with mPEG-SH; (B) Representative XPS survey spectra of QCT, QCT@PEG, QCT@CUR_0.25, and QCT@CUR@PEG NPs; (C) Sulfur content of the NPs measured by XPS. A significant increase in S 2p signals was observed after PEGylation, which further confirms surface modification of QCT@PEG and QCT@CUR@PEG NPs with mPEG-SH; (D) A significant reduction in C/O atom % ratio signifies an increase in C-O-C components on the surface of QCT@PEG and QCT@CUR@PEG NPs, consistent with PEGylation. ***$p < 0.001$; ****$p < 0.0001$.

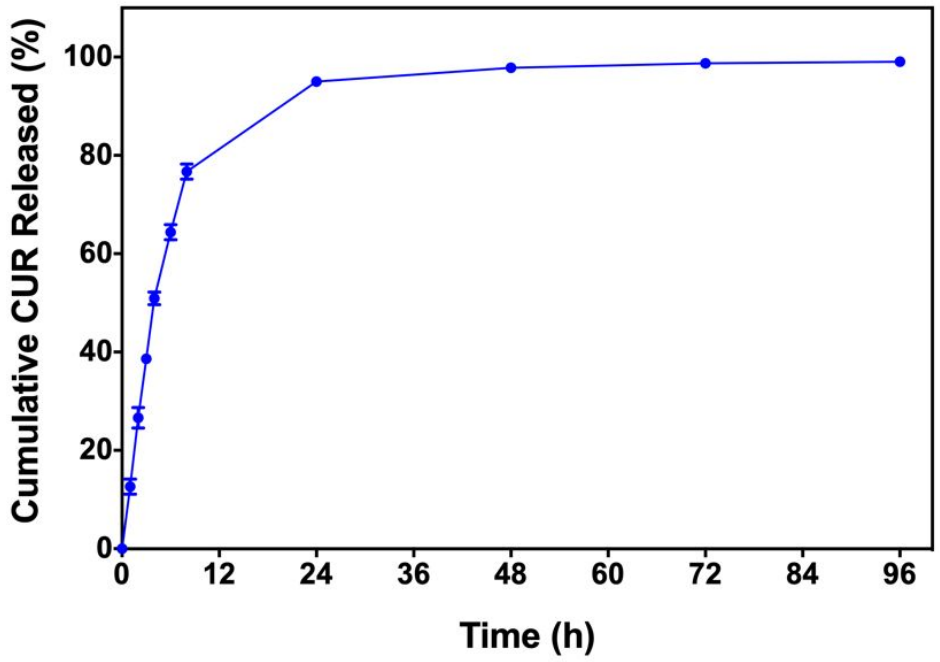

Figure 4. Cumulative release of CUR from PEGylated CUR-loaded QCT NPs (QCT@CUR@PEG NPs; n = 3) in PBS pH 7.4 showing sustained release over 4 days.

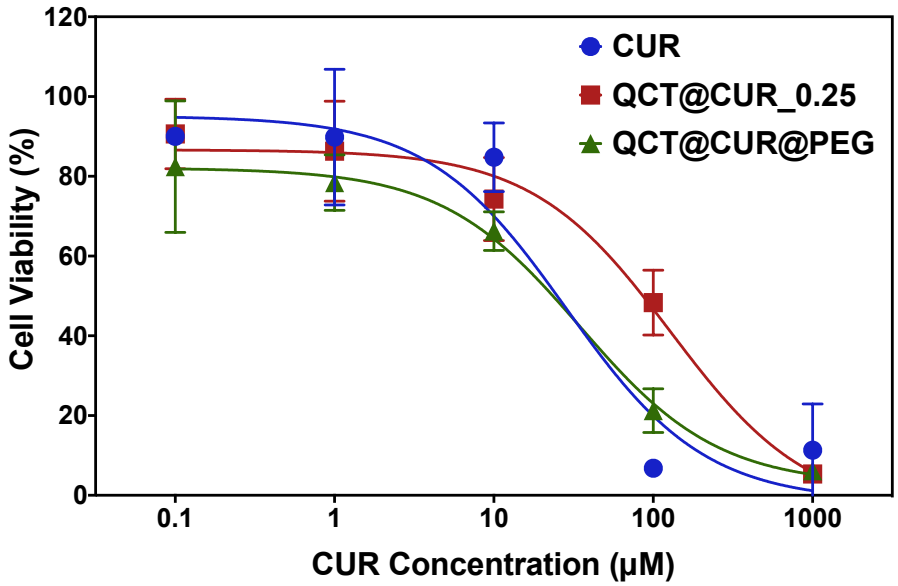

Figure 5. Cell viability of CT26 cells after 72 h incubation with 0 – 1000 μM free CUR, CUR-loaded QCT NPs (QCT@CUR_0.25 NPs), or PEGylated CUR-loaded QCT NPs (QCT@CUR@PEG NPs) (n = 4). Free CUR and QCT@CUR@PEG NPs exhibited comparable potency with an IC_{50} of 28.5 and 34.7 μM, respectively, whereas QCT@CUR_0.25 NPs showed lower potency with an IC_{50} of 128.3 μM.

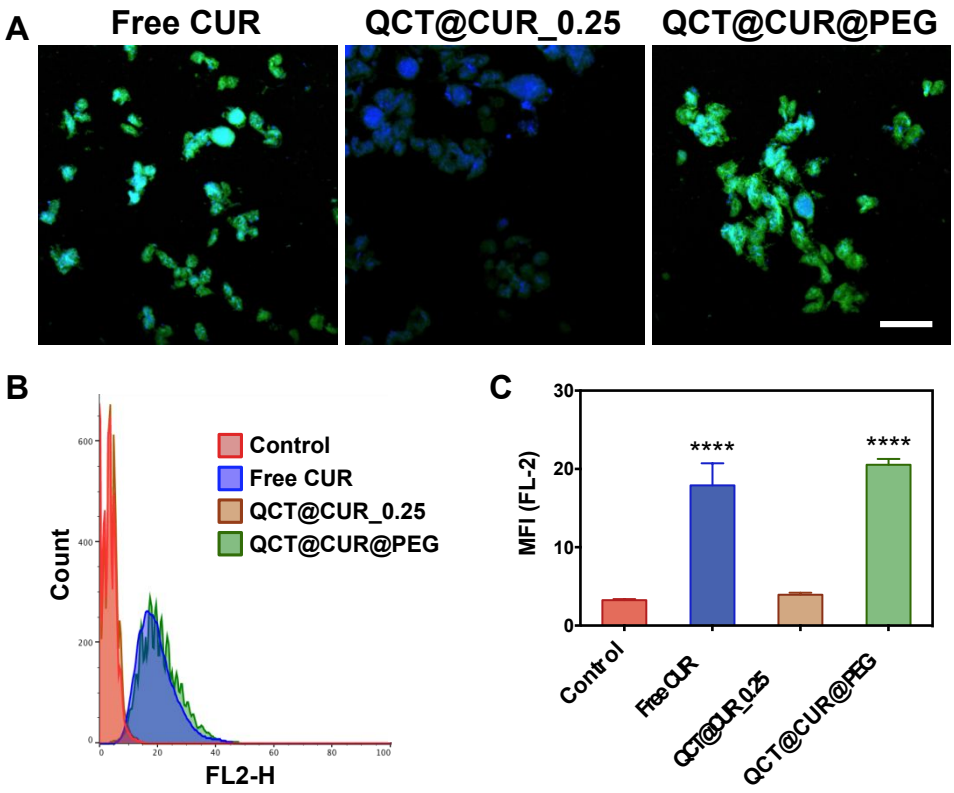

Figure 6. Cellular uptake of CUR and CUR-loaded NPs in CT26 cells. (A) Confocal microscopy images of CT26 cells treated with 20 μM free CUR, nonPEGylated CUR-loaded NPs (QCT@CUR_0.25 NPs), or PEGylated CUR-loaded NPs (QCT@CUR@PEG NPs) for 24 h. Uptake of QCT@CUR@PEG NPs was comparable to free CUR as indicated by the strong intracellular green fluorescence signals, while QCT@CUR_0.25 NPs showed much weaker fluorescence signals signifying reduced cellular uptake. Blue: cell nuclei stained by DAPI; green: CUR; scale bar = 20 μm; (B) Representative flow cytometry histograms of CT26 cells treated with CUR, QCT@CUR_0.25 NPs, or QCT@CUR@PEG NPs for 24 h (n = 3); (C) Mean fluorescence intensities (MFI) of the FL-2 channel showing significantly higher cell-associated fluorescence for cells treated with free CUR and QCT@CUR@PEG NPs, compared to untreated cells and cells treated with QCT@CUR_0.25 NPs, consistent with confocal microscopy observations. ****$p < 0.0001$.

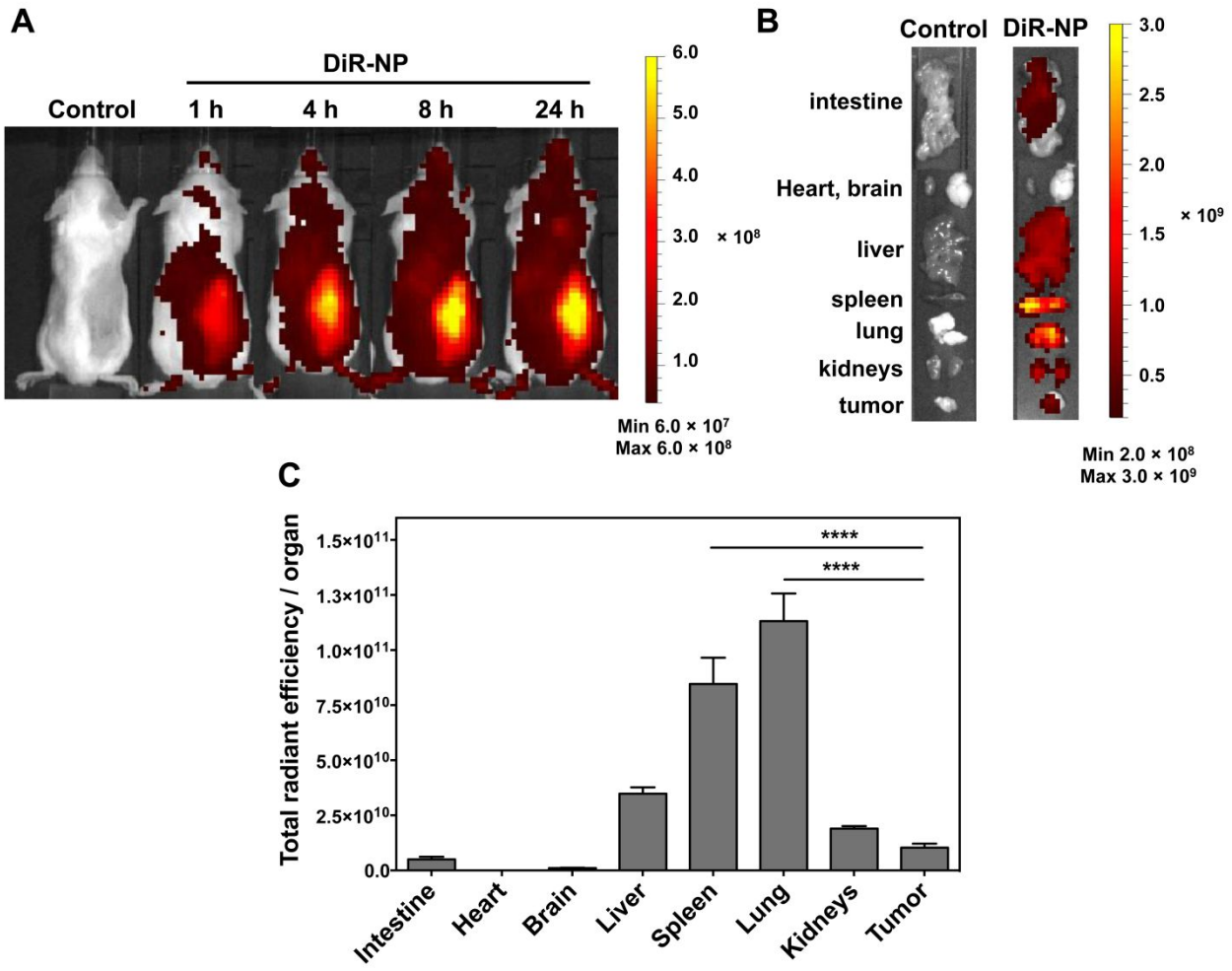

Figure 7. In vivo and ex vivo organ biodistribution of IV-administered DiR-labeled PEGylated QCT NPs (DiR-NP) in CT26 tumor-bearing Balb/c mice (n = 3). (A) Representative whole body in vivo images (dorsal view) of DiR-NP-treated animals compared to PBS-treated control obtained at 1, 4, 8, and 24 h post-injection showing a steady increase in tumor accumulation of the NPs; (B) Representative ex vivo images of excised organs at 24 h post-injection; (C) Quantified fluorescence signals of excised organs expressed as total radiant efficiency/g organ after subtracting background fluorescence. Although in vivo images showed significant accumulation of the NPs around the tumor, fluorescence intensities of excised lung and spleen were significantly higher than those of the tumors, which suggests that the NPs may still be present in the tumor vasculature at 24 h. ****$p < 0.0001$.

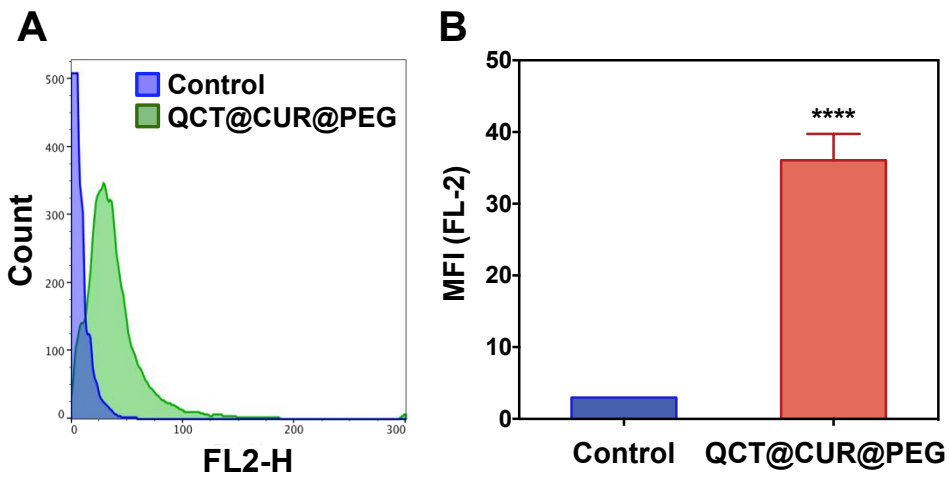

Figure 8. Tumor uptake of IV-administered PEGylated CUR-loaded NPs (QCT@CUR@PEG NPs) at 6 mg/kg CUR in CT26 tumor-bearing Balb/c mice (n = 3). Tumors were excised 30 h post-injection and tissue homogenates were analyzed by flow cytometry. (A) Representative flow cytometry histograms and (B) corresponding MFI of tumor homogenates from untreated and NP-treated animals showing significant tumor accumulation of CUR. ****$p < 0.0001$.

For Table of Contents Use Only

Bioinspired Polymerization of Quercetin to Produce a Curcumin-loaded Nanomedicine with Potent Cytotoxicity and Cancer Targeting Potential In Vivo

Suhair Sunoqrot[ab]*, Tahany Al-Debsi[a], Eveen Al-Shalabi[a], Lina Hasan[a], Farid Nazer Faruqu[b], Adam Walters[b], Robert Palgrave[c], and Khuloud T. Al-Jamal[b].

[a]*Department of Pharmacy, Faculty of Pharmacy, Al-Zaytoonah University of Jordan, Amman 11733, Jordan*

[b]*Institute for Pharmaceutical Science, King's College London, London SE1 9NH, UK*

[c]*Department of Chemistry, University College London, London WC1H 0AJ, UK*